EUROPEAN JOURNAL OF COMPUTATIONAL MECHANICS, 2016
VOL. 25, NO. 4, 309–328
http://dx.doi.org/10.1080/17797179.2016.1199237

Taylor & Francis
Taylor & Francis Group

# A new strategy for the relative movement of rough surfaces in contact using a boundary element method

Ali Ghanbarzadeh, Mark Wilson, Ardian Morina and Anne Neville

School of Mechanical Engineering, University of Leeds, Leeds, UK

**ABSTRACT**

Contact mechanics of rough surfaces is becoming increasingly important in understanding the real behaviours of machine elements in contact. Due to the complicated physical, chemical and mechanical phenomena occurring at surfaces, especially in boundary lubrication, a multiphysics numerical model is essential to capture the behaviour. Boundary Element Method is a well-known numerical approach to model such a problem because of several advantages. Firstly, it is far faster than Finite Element Method since only the boundaries of the solids are discretised. In addition, there is no problem of remeshing the contacting bodies due to plastic deformation and wear. Conventional Boundary Element models simulate movement of contacting surfaces by shifting matrices of numbers in one direction. In this new proposed approach, the big matrices of surfaces are cut into small matrices which indicate the part of surfaces that are in contact. The influence matrix is also cut into a smaller square matrix corresponding to the size of surface matrices. This approach enables matrix implications in smaller sizes than the original big surfaces and reduces the computational time.

**ARTICLE HISTORY**
Received 4 February 2016
Accepted 6 June 2016

**KEYWORDS**
Contact mechanics; boundary element method; roughness; influence matrix

## 1. Introduction

Contact mechanics which explains the behaviour of materials in contact is of great importance since it occurs almost in all mechanical machine elements. In computational mechanics, Finite Element Method is a widely used approach to solve the contact problem. Robust formulations for contact and deformation of the solids are big advantages of FEM. Since the contact of solids is multiscale in nature, a multiscale computational analysis of the contact problem is essential.

Contact mechanics studies go back to nineteenth century when Hertz (1881) developed a model for a simple elastic contact. Hertz calculated contact pressure and deformation of an elastic contact. For this purpose, a load was applied to

**CONTACT** Ali Ghanbarzadeh a.ghanbarzadeh@leeds.ac.uk

surfaces and contact mechanics analysis started. As a result of load, each surface is deformed by $u_i(x_1, x_2)$. A gap between surfaces was considered and Equation (1) should be satisfied in the contact:

$$u_1(x_1, x_2) + u_2(x_1, x_2) + g(x_1, x_2) = \delta_1 + \delta_2 \tag{1}$$

Hertz calculated the contact pressure of $p(x_1, x_2)$ in the case of satisfying the above equation.

Surfaces are rough in reality and contact of rough surfaces is more complicated than the Hertzian contact of flat surfaces. Because of the small scale of the roughness of the surfaces in comparison to the bulk of the solids, Finite element Analysis of such a problem becomes cumbersome. One of the first attempts to mathematically solve the contact of rough surfaces was the work of Greenwood and Williamson (1966). They used the probabilistic approach to predict the contact between surface asperities and determined the real area of contact. That model of contact mechanics was a starting point for understanding the real stochastic behaviour of surface asperities in contact. Despite the abilities of the model, it had no deterministic capabilities for measured surface topography.

Deterministic contact mechanics models have been the subject of many studies in the past few years to consider the true interaction of surface asperities in contact. Attempts were made on simulating the contact of surfaces using Finite Element Method. Bortoleto, Rovani, Seriacopi, Profito, and Zachariadis (2012) simulated a single ball-on-disc experiment by the finite element method and used Archard's wear equation to simulate wear. They validated the simulation results with experiments and showed good agreement. Öqvist (2001) also used a finite element model to simulate a contact and implemented Archard's wear to calculate wear using an updated geometry with different step sizes.

Hegadekatte, Hilgert, Kraft, and Huber (2010) developed a multi-time-scale model for wear prediction in micro gear application. They used commercial codes for determining their contact pressure and deformations and then used Archard's wear equation for calculating wear. The problem of meshing size and remeshing the geometry was addressed in that work, especially for the case of macro component wear calculations. Sellgren, Björklund, and Andersson (2003) incorporated random rough surfaces into Finite Element analysis and calculated the true area of contact. They concluded that Finite Element method can predict the real area of contact for rough surfaces. This prediction depends on the amplitude and wavelength properties of the interacting surfaces.

Boundary Element Method is also widely used for simulating the contact mechanics problem due to its efficiency. Sfantos and Aliabadi (2006a, 2006b, 2007), developed boundary element simulations to calculate wear in sliding wear conditions. They reported that BEM is an efficient method for contact calculation of surfaces. They also used BEM for simulating the three-dimensional sliding wear and validated the model with an artificial hip joint wear simulator.

Ilincic et al. (2011, 2013); Ilincic, Vorlaufer, Fotiu, Vernes, and Franek (2009) used the Boundary Element Method and also a combined boundary-finite element method to simulate wear in tribometers using localised Archard's wear. They predicted the shape of the wear track of a flat surface in a reciprocating pin-on-disc tribometer using BEM. Andersson, Almqvist, and Larsson (2011) used a wear model and implemented FFT-based contact mechanics simulations to calculate contact pressure and deformations. They simulated a ball-on-disc wear experiment and validated their simulation results with experiments.

There are several other works that simulate contact mechanics of rough surfaces using the Boundary Element Method for predicting wear and micropitting in rolling and rolling–sliding conditions (Bosman & Schipper, 2011a, 2011b; Morales-Espejel & Brizmer, 2011). All these numerical procedures confirm that BEM is a suitable method for simulating contact mechanics.

Movement of surfaces are essential parts of any contact mechanics model that simulates sliding, rolling or sliding–rolling of contacting surfaces. In this work, a new numerical approach for movement of surfaces in contact mechanics simulations in Boundary Element Method is introduced. Instead of shifting the matrices containing the surface asperity height values, those parts of surfaces that come into contact are selected for contact mechanics simulation. The influence matrix is also modified with respect to the size of the part of the surfaces that are in contact. This approach helps to have smaller influence matrices and will increase the computational efficiency by several times. The details of the contact mechanics used in the Boundary Element simulation are also reported in this work. The contact mechanics model introduced in this work was used to investigate a boundary lubricated contact and tribochemistry in other works by the authors (Ghanbarzadeh, Wilson, Morina, Dowson, & Neville, 2016; Ghanbarzadeh, Parsaeian, et al., 2016; Ghanbarzadeh, Piras, et al., 2016) and the predicting capability of the model was tested. In this paper, firstly, the components of the contact mechanics model are introduced in Section 2. The new strategy for the movement of the surfaces based on the new mathematical algorithm is presented in Section 2.5.1. Then some examples of the results of the evolution of the asperity contact pressure are shown in Section 3.

## 2. Components of the model

### *2.1. Rough surface generation*

To study the contact of rough surfaces deterministically, digitised surfaces should be used as inputs into the model. There are two different ways of digitising surfaces. The first way is to use surface microscopes such as Atomic Force Microscope which can give a three-dimensional digitised map of the surface topography. Alternatively, surfaces can be generated using mathematical methods. The method used to generate surfaces is introduced by Tonder and Hu (1992).

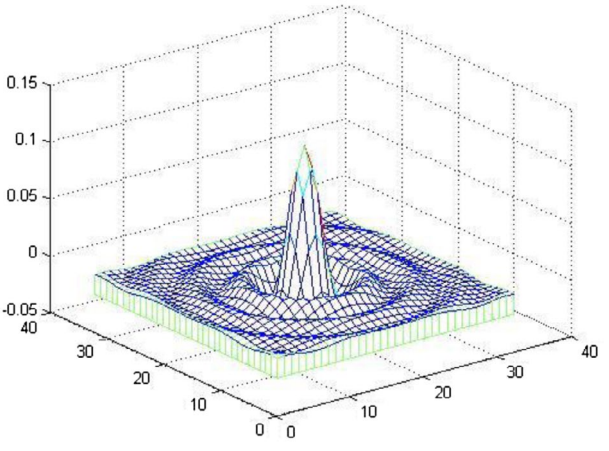


**Figure 1.** Filter coefficient for a circular digital low-pass filter.

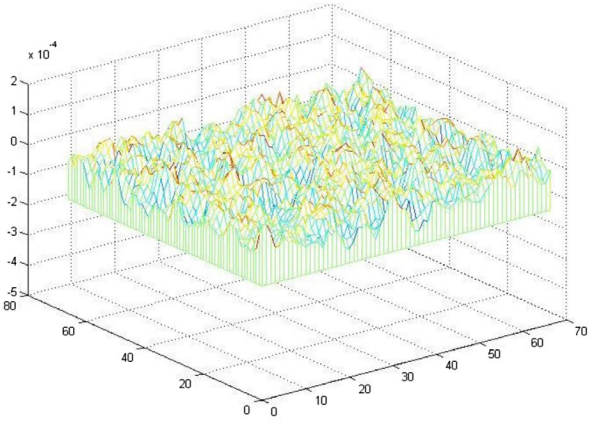


**Figure 2.** Three-dimensional digital rough surface generated using low-pass filter and random Gaussian numbers.

For generation of three-dimensional rough surfaces, a specific autocorrelation factor and also height distribution should be defined. Two-dimensional digital filters are used for generating the three-dimensional surfaces. By using random number generators, it is possible to generate the filter inputs as Gaussian-independent random numbers. The output would be obtained through the filtering operation and will give the sequence with certain autocorrelation function. It is mathematically proved that if the input numbers are Gaussian random numbers, the distribution will remain Gaussian after the filtering. The filtering coefficient for generating the rough surfaces is plotted in Figure 1. An example of three-dimensional digitised rough surface is shown in Figure 2.

This method enables varying surface roughness for studying the effect of roughness on contact of surfaces. As discussed before, surface roughness is very important in contact of surfaces in different scales; therefore, this generation method

gives the flexibility to generate different desired surfaces and investigating the surface effects in boundary lubrication.

### 2.2. Contact of rough surfaces

There have been many attempts at simulating the contact of rough surfaces in contact mechanics (Almqvist, Sahlin, Larsson, & Glavatskih, 2007; Bhushan, 1998; Borri-Brunetto, Chiaia, & Ciavarella, 2001; Conry & Seireg, 1971; Ilincic et al., 2009, 2011, 2013; Kalker & Van Randen, 1972; Lai & Cheng, 1985; Poon & Sayles, 1994; Ren & Lee, 1993; Sellgren et al., 2003; Thomson & Bocchi, 1972; Webster & Sayles, 1986). The contact mechanics model developed by Tian and Bhushan (1996) which considers the complementary potential energy will be used in this work. By applying the Boussinesq method (Johnson, 1987) and relating the contact pressures to surface deformations, the problem would be to solve the contact mechanics only for finding contact pressures at each node and then the related contact deformations can be calculated. For this model, surfaces should be discretised into small nodes and it is assumed that the nodes are small enough and the contact pressure is constant at each node.

The problem is to minimise the complementary potential energy as follows:

$$V^* = \frac{1}{2}\iint p\bar{u}_z \mathrm{d}x\mathrm{d}y - \iint p\ \bar{u}_z^* \,\mathrm{d}x\mathrm{d}y \tag{2}$$

where $p$ is the contact pressure and $V^*$, $\bar{u}_z$ and $\bar{u}_z^*$ are complementary potential energy, surface deformation and prescribed displacement, respectively.
The Boussinesq solution for relating contact pressure and surface deformation usually considers only normal forces and the solution is:

$$u(x,y) = \frac{1}{\pi E^*}\int_{-\infty}^{\infty}\int \frac{p(s_1,s_2)}{\sqrt{(x-s_1)^2+(y-s_2)^2}} ds_1 ds_2 \tag{3}$$

in which $E^*$ is the composite elastic modulus of two surfaces. $(x, y)$ and $(s_1, s_2)$ are two different surface points. It shows the relationship for the deformation of the surface on point $(x, y)$ when the load is applied on the point $(s_1, s_2)$.

$$\frac{1}{E^*} = \frac{(1-\nu_1^2)}{E_1} + \frac{(1-\nu_2^2)}{E_2} \tag{4}$$

$$\frac{1}{G^*} = \frac{(1+\nu_1)(1-2\nu_1)}{2E_1} - \frac{(1+\nu_2)(1-2\nu_2)}{2E_2} \tag{5}$$

here, $\nu_1$, $\nu_2$, $E_1$ and $E_2$ are the Poisson ratio and Elastic Modulus of surfaces 1 and 2, respectively.

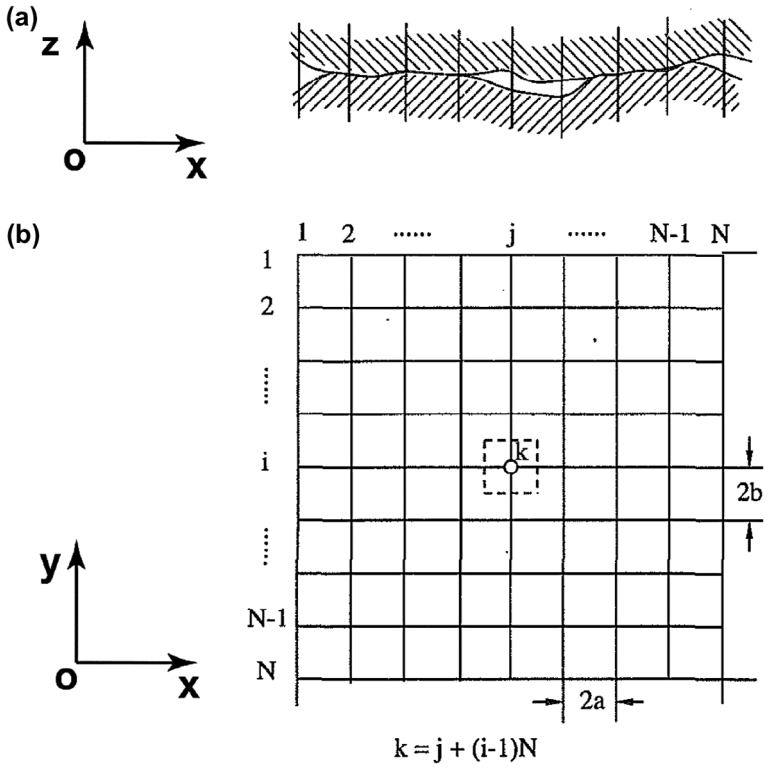


**Figure 3.** Surface discretisation in Boundary Element Method (Reprinted from Tian and Bhushan (1996).

For solving the double integrals of Equation (3) the surfaces should be discretised into small nodes. The nodes should be small enough to assume that pressure is constant at each node. It should be noted that only boundary of solids (surfaces) are meshed in this method which can improve numerical efficiency.

An example of the surface discretisation is shown in Figure 3.

*N* and *M* are the number of nodes in two dimensions of the surface plane and *a* and *b* are the half length of each element which is the difference between the nodes. For simplicity, *a* and *b* are assumed to be equal and in this work, they are set to .5 μm. Therefore, the full length of each element is 1 μm which is a reasonable length for computational studies of rough surfaces (Andersson, Larsson, Almqvist, Grahnb, & Minami, 2012).

To solve the integral equation for the discretised surfaces, the integral equations should first be discretised.

$$\left(\bar{u}_z\right)_l * = \frac{1}{\pi E^*} \int_0^L \int_0^L \frac{p\left(s_1, s_2\right) ds_1 ds_2}{\sqrt{\left(s_1 - x\right)^2 + \left(s_2 - y\right)^2}} \tag{6}$$

$$= \frac{1}{\pi E^*} \sum_{k=1}^{M} \iint \frac{ds_1 ds_2}{\sqrt{\left(s_1 - x\right)^2 + \left(s_1 - y\right)^2}} p_k = \sum_{k=1}^{M} C_{kl} p_k$$

where $C_{kl}$ is the influence matrix and is calculated by solving the double integral:

$$C_{kl} = \frac{1}{\pi E^*} \iint_{-\infty}^{\infty} \frac{ds_1 ds_2}{\sqrt{\left(x - s_1\right)^2 + \left(y - s_2\right)^2}} \tag{7}$$

The solution for the influence matrix in discretised form is as follows:

$$\begin{aligned} C_{kl} = \frac{1}{\pi E^*} \Bigg\{ & (x+a) \ln \left[ \frac{\left(y+b\right) + \sqrt{\left(y+b\right)^2 + (x+a)^2}}{\left(y-b\right) + \sqrt{\left(y-b\right)^2 + (x+a)^2}} \right] \\ & + \left(y+b\right) \ln \left[ \frac{(x+a) + \sqrt{\left(y+b\right)^2 + (x+a)^2}}{(x-a) + \sqrt{\left(y+b\right)^2 + (x-a)^2}} \right] \\ & + (x-a) \ln \left[ \frac{\left(y-b\right) + \sqrt{\left(y-b\right)^2 + (x-a)^2}}{\left(y+b\right) + \sqrt{\left(y+b\right)^2 + (x-a)^2}} \right] \\ & + \left(y-b\right) \ln \left[ \frac{(x-a) + \sqrt{\left(y-b\right)^2 + (x-a)^2}}{(x+a) + \sqrt{\left(y-b\right)^2 + (x+a)^2}} \right] \end{aligned} \tag{8}$$

in which $a$ and $b$ are the half length of each small element and $M$ is the total number of nodes.

Equation (2) describes the potential energy for a frictionless contact and the normal force is the only force applied on the surfaces. The potential equation for a frictional contact would be modified to the form below:

$$V^* = \frac{1}{2} \iint t\bar{u} \mathrm{d}x\mathrm{d}y - \iint t\overline{u^*}\, \mathrm{d}x\mathrm{d}y \tag{9}$$

in which $t$ is the full surface stress vector including the in-plane tractions and $u$ is the full surface deformation.

$$\boldsymbol{t} = q_x \boldsymbol{e}_x + q_y \boldsymbol{e}_y + p\boldsymbol{e}_z \tag{10}$$

$$\boldsymbol{u} = u_x \boldsymbol{e}_x + u_y \boldsymbol{e}_y + u_z \boldsymbol{e}_z \tag{11}$$

$q_x$ and $q_y$ are the in-plane traction forces and $\boldsymbol{ex}$, $\boldsymbol{ey}$ and $\boldsymbol{e}_z$ are the Cartesian unit basis vectors. $u_x$, $u_y$ and $u_z$ are the surface deformations in $x$, $y$ and $z$ directions, respectively.

By applying the same discretising procedure, the Boussinesq solution for the fully coupled deformation–traction relationship can be expressed as:

$$u_{xk} = \sum_{l=1}^{M} \left( C_{kl}^{xx} q_{xl} + C_{kl}^{xy} q_{yl} + C_{kl}^{xz} p \right)$$

$$u_{yk} = \sum_{l=1}^{M} \left( C_{kl}^{yx} q_{xl} + C_{kl}^{yy} q_{yl} + C_{kl}^{yz} p \right) \tag{12}$$

$$u_{zk} = \sum_{l=1}^{M} (C_{kl}^{zx} q_{xl} + C_{kl}^{zy} q_{yl} + C_{kl}^{zz} p)$$

In the matrix form:

$$\begin{bmatrix} u_x \\ u_y \\ u_z \end{bmatrix} = \begin{bmatrix} C^{xx} & C^{xy} & C^{xz} \\ C^{yx} & C^{yy} & C^{yz} \\ C^{zx} & C^{zy} & C^{zz} \end{bmatrix} \begin{bmatrix} q_x \\ q_y \\ p \end{bmatrix} \tag{13}$$

The elements of the influence matrix can be obtained from the complete solution of the Boussinesq problem. Then the problem would be minimising the potential energy for the fully coupled contact. The solution procedure is the same as frictionless contact and can be carried out by direct quadratic mathematical solution (Tian & Bhushan, 1996; Willner, 2008).

For the case of two identical materials in contact, the equivalent shear modulus of Equation (5) becomes zero and the Equation (9) reduces to Equation (3).

### 2.3. Direct quadratic mathematical programming

Because the total complementary potential energy is a quadratic function of the contact pressure, it can be expressed as quadratic mathematical equations. Hence, the energy can be written in quadratic form of Equation (14):

$$V^* = \frac{1}{2} p^T . C . p - p^T u \tag{14}$$

here $p^T$ is the transpose matrix of $p_k$ and $C$ and $u$ are influence matrix and gap between surfaces, respectively.

$$C = \frac{1}{\pi E^*} \begin{bmatrix} C_{1,1} & \cdots & C_{1,M} \\ \vdots & \ddots & \vdots \\ C_{M,1} & \cdots & C_{M,M} \end{bmatrix} \tag{15}$$

$$u^T = (\overline{\overline{u^*_{z1}}, \overline{u^*_{z2}}, \ldots, \overline{u^*_{zk}}, \ldots, \overline{u^*_{zM}}}) \tag{16}$$

And for the complementary potential energy to have a minimum at the point $p^*$, the solution is as:

$$\nabla V^*(p^*) = C.p^* - u = 0 \tag{17}$$

$$p^* = C^{-1}.u \tag{17}$$

And all the values in Equation (17) should satisfy the restriction criteria $p_k \geq 0$. The summation of all contact pressures must be equal to the applied load on the surfaces and the following equation should be satisfied:

$$\sum_{i,j=1}^{i,j=N} p_{i,j} = W \tag{18}$$

The elastic deformation is then calculated corresponding to the pressure of contacting asperity using the equation below:

$$u = C.p \tag{19}$$

The deformation is then used to check the deformation criteria of the contact problem. It should be noted that Equation (18) will be valid for the whole contact. In order to find the true area of contact and the corresponding contact pressures, Equations (18) and (20) should be solved at the same time iteratively.

The rigid body movement ($r$) is the movement of the bodies in normal direction of contact and is given by:

$$r = (Z_2 - Z_1) + u \,\&\, p > 0 \quad \text{if in contact} \tag{20}$$

$$r < (Z_2 - Z_1) + u \,\&\, p = 0 \quad \text{if not in contact}$$

in which $(Z_2 - Z_1) = g$ is the gap between asperities and u is the elastic deformation of contacting asperities. The above formulations are valid for every single asperity in contact. Therefore, they can be solved for a set of asperites and Figure 4 can be a representative of a single node in the contact mechanics formulation of the problem explained in Figure 3.

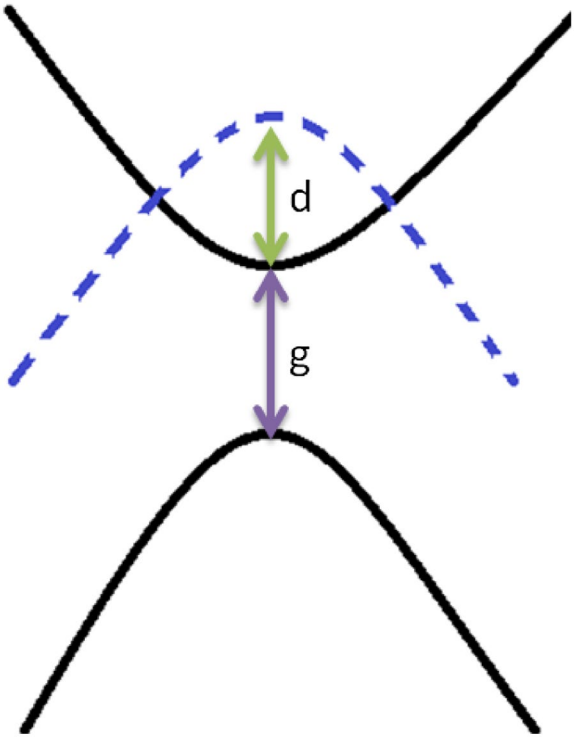


**Figure 4.** Single asperity model – Schematics of rigid body movement.

### *2.4. Elastic–perfectly plastic contact model*

The contact mechanics model used in this work is an elastic–perfectly plastic model. To consider the plastic part in the simulation, a modelling approach which was reported by Sahlin, Larsson, Almqvist, Lugt, and Marklund (2009) was used in this work. It is assumed that the asperities can undergo pressures between 0 and hardness of the materials:

$$0 < p(x, y) < H \tag{21}$$

The contact pressure of the asperities that experience pressures higher than the hardness of the materials will be set to H (hardness of the material).

These asperities become plastically deformed. It is assumed that the points with pressures equal to the hardness of the material will be truncated out of the calculation for elastic deformation because they can freely float. The steps for elasto-plastic contact simulation are explained as below:

- First step is to guess the initial pressure to satisfy Equation (18).
- Set the negative pressures to zero and the pressures above the hardness to H
- Check the calculated pressures again and compare it with Equation (18). If the pressure is now equal to load, pressures should be shifted up or down

- Truncate the pressures $p = 0$ and $p = H$. Then calculate the elastic deformation of Equation (19).
- Calculate the body interferences and check if the points of contact will satisfy Equation (20).
- The plastic deformation is then calculated by subtracting the elastic deformation from the body interferences.

### 2.5. Movement of the contacting surfaces

The influence matrix of Equation (15) shows the influence of surface points on deformation of other points in presence of load. The term g which is a two-dimensional matrix of gaps between single asperities of contacting surfaces, shows the potential of asperity–asperity contact by moving surfaces in normal direction of surface planes. In this case, Equation (20) defines the possibility of contact to happen.

In most of the tribologically loaded contacts, surfaces have relative movements tangentially, so this must be taken into account. Conventionally, movement of surfaces are applied by shifting the matrices that contain the surface asperity height numbers. This is a very simple way to simulate the movement of surfaces. In this method, controlling the shifting speed of both contacting surfaces is essential for applying the rolling–sliding condition on the tribosystem.

The influence matrix does not change in this method and the size is still $(N * M) \times (N * M)$ which in the case of square contacting area becomes $N^2 \times N^2$.

#### 2.5.1. New surface movement strategy

It is important to know how the influence matrix works before explaining the new procedure for moving the surfaces. The elements of an influence matrix correspond to the influence of a node of surface on other nodes of the surface if the load is applied on that point.

Imagine a surface with $N \times N$ nodes. If the load is applied to a point, it influences $N \times N$ points on the surfaces including the point itself. Therefore, a matrix of $N^2 \times N^2$ can explain the influence matrix of the whole surface. Each element of this matrix is responsible for the influence of a point on another point (Figure 5). If the load is applied on point $p$, it will affect the deformation on point $k$.

It can be interpreted from Equation 8 that the elements of this matrix are dependent on the distance of the points on the surface (distance between points $p$ and $k$). Therefore, this matrix would have identical values for the points that have similar distances.

Now imagine two surfaces coming into rolling–sliding contact. One of the surfaces should enter the contact from one side and will exit the contact on the opposite.

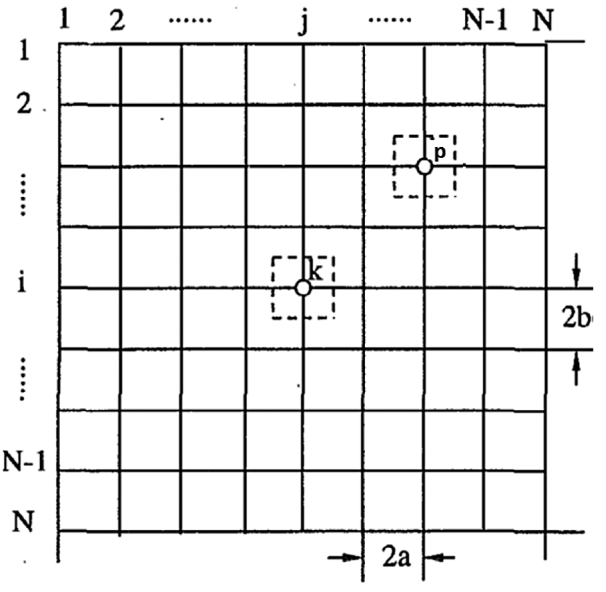


**Figure 5.** Discretised surface and influence matrix definition.

If the upper surface enters the contact from the left, its rightmost part would be in contact with the leftmost part of the lower surface (Figure 6(b)). Then the contact problem reduces to the contact of two one-dimensional matrices of two surfaces with size ($\boldsymbol{N \times 1}$). When the movement continues, more points of surfaces come into contact. For example, two columns of the rightmost points of upper surface come into contact with two columns of the leftmost points on the lower surface (Figure 6(c)). This process continues until the surfaces fully come into contact and the upper surface exits the contact from the other side. A schematic of this contact process is shown in Figure 6.

For the beginning of the contact, one column of each surface comes into contact. In this case, the influence matrix needs to cover the contact of $N$ points on one surface with N points on another surface. Therefore, the influence matrix only needs to be the first $N \times N$ matrix of the big $N^2 \times N^2$ influence matrix. It is shown in Figure 7 that how this $N \times N$ matrix is selected.

The true influence matrix elements should satisfy Equation 8. As stated before, these elements are dependent on the distance of the points of the surface so the selection shown in Figure 7 is valid.

If the movement continues and more points of the surfaces come into contact, the influence matrix will get bigger and becomes $2N \times 2N$, $3N \times 3N$, … and $N^2 \times N^2$ at the end when surfaces are completely in contact.

The problem of contact becomes faster because the size of matrices of surfaces and influence matrices are much smaller in this case. The maximum size of the influence matrix is when two surfaces are in complete contact and it is the same size as conventional shifting of surfaces. It should be noted that the rigid body

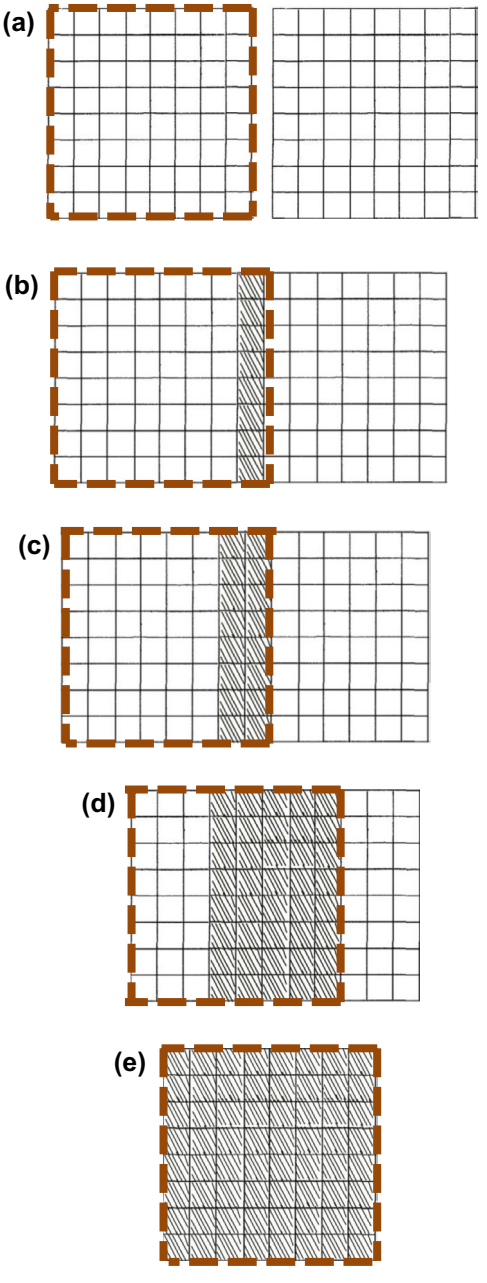


**Figure 6.** Movement of surfaces in contact. The shaded area shows the area of contact between two surfaces. The red dotted lines show the area of the upper surface that enters the contact from the left. (a) Two surfaces not in contact yet, (b) Start of the contact (rightmost part of a surface in contact with leftmost part of another surface), (c) Two surfaces come into contact by more areas of both surfaces, (d) More evolution in the contact area of surfaces, and (e) Entire surfaces are in contact.

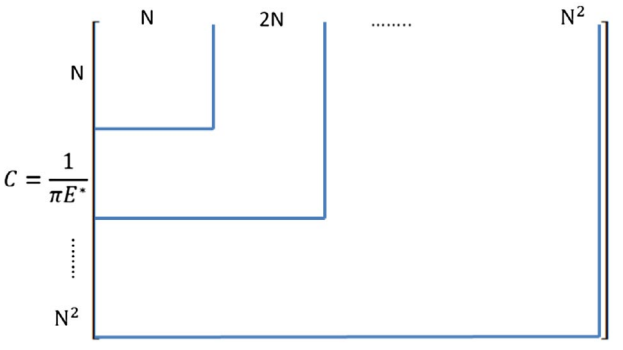


**Figure 7.** Influence matrix selection in the case of moving surfaces.

movement ($r$) is set as constant in one entire step of the contact calculation (from when the surfaces come into the contact up until the surfaces exit the contact). The average of the surface contact pressures are taken in one step and this value is used to satisfy Equation (18). In this case, upper surface is passed relative to the lower surface and the average of the contact pressure is calculated on surface asperities and the calculation is iterated until it satisfies Equations (18) and 20.

Then the contact pressures and surface deformations are stored for every step and can be averaged for one loading cycle. Plastic deformations are applied to the surface asperities and the geometries of the surfaces are changed for next steps. This process of two rough surfaces coming into contact is repeated to the end of the simulation. Therefore, a rolling–sliding motion can be easily modelled by this contact mechanics simulation. It should be noted that the contact mechanics model in this work is quasi-static.

## 3. Results and discussion

Results for influence matrix and contour of contact pressure for movement of surfaces are reported in this section.

### *3.1. Influence matrix*

As explained before, influence matrix is $N^2 \times N^2$ when the surfaces are $N \times N$. An example of influence matrix for a $20 \times 20$ surface is shown in Figure 8.

If load is applied to a point of this surface, the deformation on all the other points is shown in Figure 9.

It is noticeable that if a load is applied to a certain point on the surface, the highest deformation happens at the same point and this deformation decreases as the distance from that point increases. It is in agreement with the definition of the influence matrix.

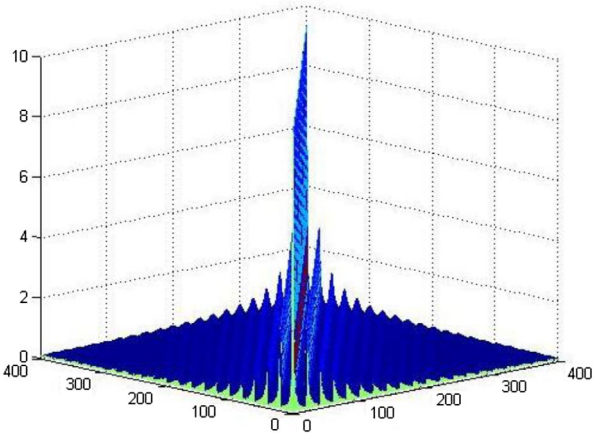


**Figure 8.** Influence matrix element values.

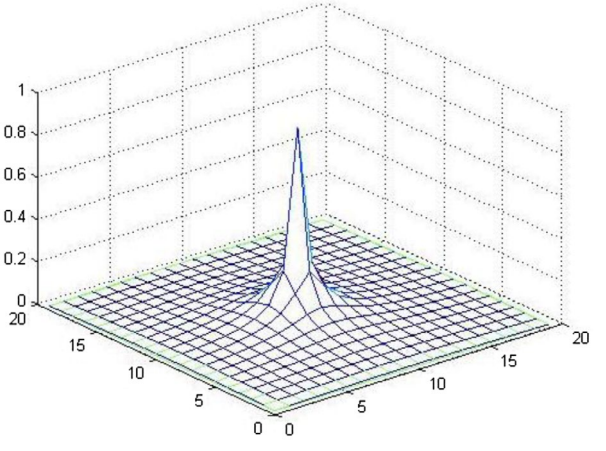


**Figure 9.** The deformation of surface due to load applied in the centre.

Figure 8 shows the elements of influence matrix and it approves the fact that selection of matrix elements based on Figure 7 is valid. By selecting the first $N \times N$ matrix of the large $N^2 \times N^2$ influence matrix, the influence of one point of the surface on the 20 points of the same column is selected. That is for the case that surfaces are only at the beginning of the contact.

It can be also noted that the influence matrix of Figure 8 is diagonal which means that the influence element of all points are the same on themselves and is reduced by the distance of the points from each other. It is also symmetric diagonally which means that the same distance between the points results in the same influence value.

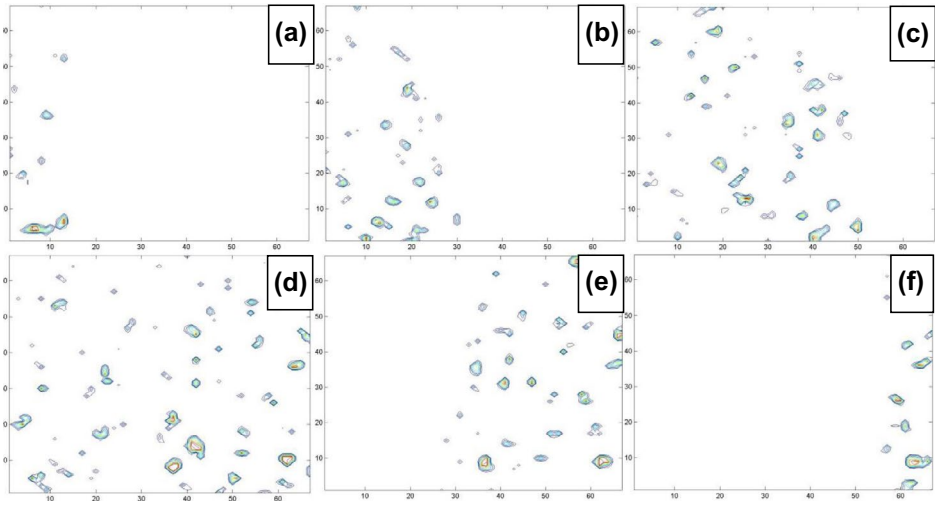


**Figure 10.** Contour of contact pressure showing the asperity contact pressures in surface movement. The upper surface enters the contact from the left (a) and exits from the right (f). The contour indicates the pressures on the lower body.

### 3.2. Movement of the surfaces

As explained in Section 2.5 matrices of surfaces are selected in a way that movement can be simulated. An example of this movement is shown in Figure 10. The contour of contact pressure which shows the asperity–asperity interaction is demonstrated in the figure. The evolution of contacting asperities in the sliding direction can be noticed from the figure.

The upper surface comes into contact with lower surface from the left (see Figure 10(a)) and moves towards the sliding direction. Both surfaces are entirely in contact in Figure 10(d). The upper surface then exits the contact from the other side (Figure 10(f)).

The influence matrix is smaller in the beginning of the contact (Figure 10(a)) and increases in size whilst more surface points come into contact. It gets the size of the original influence matrix whilst two surfaces are completely in contact (Figure 10(d)) and then reduces in size as the upper surface start to exit the contact.

### 3.3. Application in non-linear contact problems

Non-linear contact problems have been the subject of many studies. Models focused on incorporating non-linear behaviour in finite element methods, boundary element methods and combination of them two (Andersson, 1981; Ezawa & Okamoto, 1995; Kosior, Guyot, & Maurice, 1999; Landenberger & El-Zafrany, 1999; Liu, Zhu, Yu, & Wang, 2001; Man, Aliabadi, & Rooke, 1993a, 1993b; Olukoko, Becker, & Fenner, 1993; Oysu & Fenner, 1998; Yamazaki, Sakamoto, & Takumi, 1994).

Any contact problem will be no longer a linear one due to yielding of the materials in contact. The stress can be calculated at any loading increment as the following:

$$[\Delta\sigma] = \left[D_{ep}\right].[\Delta\varepsilon] \tag{22}$$

where $[\Delta\varepsilon]$ is the strain increment and $[D_{ep}]$ is the elasto-plastic influence matrix. It is shown numerically that the stress fields and the contact deformations in an elasto-plastic non-linear problem can be calculated using the influence matrices used for elastic problems with a more complicated numerical algorithm (Liu et al., 2001). Results show that calculation of non-linear problems need the influence matrix or the stiffness matrix for pressure/deformation calculations. However, these numerical results are for the contact of material in a normal loading without any tangential movements. Therefore, the movement methodology shown in Section 2.5.1 is applicable for movement of surfaces in the case of non-linear contact problems. The only change in the numerical approach would be adapting the influence/stiffness matrices to account for the part of the surfaces that are in contact.

## 4. Conclusion

Boundary Element Method is an efficient approach for simulating the contact mechanics especially in the case of rough surfaces. Tribological contacts are dynamic and surfaces are in relative motion in contact. These dynamic conditions will result in modification to geometry and physics of the contacting bodies. Modelling such a problem needs a robust and efficient algorithm for movement of surfaces. A new algorithm for movement of surfaces in Boundary Element Method was reported in this work. In this approach, parts of the surfaces are selected out of the bigger real area of contact and the corresponding influence matrix is extracted from the original influence matrix. A big advantage of this approach is the smaller sizes of influence matrix for contacts. The computation time of a contact mechanics simulation is directly proportional to size of the influence matrix. The contact mechanics results shown in this work are similar to the ones reported in the literature. This approach can be also used for the non-linear contact problems by adapting the influence/stiffness matrices in a way that only account for the part of the surface that are in contact. Influence/stiffness matrices can be modified for each loading increments in the non-linear problem. Smaller matrices can increase the efficiency of the non-linear problems by several times.

## Disclosure statement

No potential conflict of interest was reported by the authors.

## Funding

This work was supported by the FP7 programme through the Marie Curie Initial Training Network (MC-ITN) entitled 'ENTICE – Engineering Tribochemistry and Interfaces with a Focus on the Internal Combustion Engine' [290077] and was carried out at University of Leeds.

## References

Almqvist, A., Sahlin, F., Larsson, R., & Glavatskih, S. (2007). On the dry elasto-plastic contact of nominally flat surfaces. *Tribology International, 40*, 574–579.

Andersson, T. (1981). The boundary element method applied to two-dimensional contact problems with friction. In *Boundary element methods*. (pp. 239–258). Heidelberg: Springer.

Andersson, J., Almqvist, A., & Larsson, R. (2011). Numerical simulation of a wear experiment. *Wear, 271*, 2947–2952.

Andersson, Joel, Larsson, Roland, Almqvist, Andreas, Grahnb M., & Minami, I. (2012). Semi-deterministic chemo-mechanical model of boundary lubrication. *Faraday Discussions, 156*, 343–360.

Bhushan, B. (1998). Contact mechanics of rough surfaces in tribology: Multiple asperity contact. *Tribology Letters, 4*(1), 1–35.

Borri-Brunetto, M., Chiaia, B., & Ciavarella, M. (2001). Incipient sliding of rough surfaces in contact: A multiscale numerical analysis. *Computer Methods in Applied Mechanics and Engineering, 190*, 6053–6073.

Bortoleto, E. M., Rovani, A. C., Seriacopi, V., Profito, F. J., Zachariadis, D. C., Machado, I. F., … Souza, R. M. (2012). Experimental and numerical analysis of dry contact in the pin on disc test. *Wear, 301*, 19–26.

Bosman, R., & Schipper, D. J. (2011a). Mild wear prediction of boundary-lubricated contacts. *Tribology Letters, 42*, 169–178.

Bosman, R., & Schipper, D. J. (2011b). Running-in of systems protected by additive-rich oils. *Tribology Letters, 41*, 263–282.

Conry, T. F., & Seireg, A. (1971). A mathematical programming method for design of elastic bodies in contact. *Journal of Applied Mechanics, 38*, 387–392.

Ezawa, Y., & Okamoto, N. (1995). Development of contact stress analysis programs using the hybrid method of FEM and BEM. *Computers & structures, 57*, 691–698.

Ghanbarzadeh, A., Parsaeian, P., Morina, A., Wilson, M. C., van Eijk, M. C., Nedelcu, I., … Neville, A. (2016). A semi-deterministic wear model considering the effect of zinc dialkyl dithiophosphate tribofilm. *Tribology Letters, 61*(1), 1–15.

Ghanbarzadeh, A., Piras, E., Nedelcu, I., Brizmer, V., Wilson, M. C. T., Morina, A., … Neville, A. (2016). Zinc dialkyl dithiophosphate antiwear tribofilm and its effect on the topography evolution of surfaces: A numerical and experimental study. *Wear*. doi:10.1016/j.wear.2016.06.004

Ghanbarzadeh, A., Wilson, M., Morina, A., Dowson, D., & Neville, A. (2016). Development of a new mechano-chemical model in boundary lubrication. *Tribology International, 93*, 573–582.

Greenwood, J. A., & Williamson, J. B. P. (1966). Contact of nominally flat surfaces. *Proceedings of the Royal Society of London A Mathematical and Physical Sciences, 295*, 300–319.

Hegadekatte, V. Hilgert, J. Kraft, O., & Huber, N. (2010). Multi time scale simulations for wear prediction in micro-gears. *Wear, 268*, 316–324.

Hertz, H. (1881). On the contact of elastic solids. *Journal für die reine und angewandte Mathematik, 92*, 156–171.

Ilincic, S., Tungkunagorn, N., Vernes, A., Vorlaufer, G., Fotiu, P., & Franek, F. (2011). Finite and boundary element method contact mechanics on rough, artificial hip joints. *Proceedings of the Institution of Mechanical Engineers, Part J: Journal of Engineering Tribology, 225*, 1081–1091.

Ilincic, S., Vernes, A., Vorlaufer, G., Hunger, H., Dorr, N., & Franek, F. (2013). Numerical estimation of wear in reciprocating tribological experiments. *Proceedings of the Institution of Mechanical Engineers, Part J: Journal of Engineering Tribology, 227*, 510–519.

Ilincic, S., Vorlaufer, G., Fotiu, P., Vernes, A., & Franek, F. (2009). Combined finite element-boundary element method modelling of elastic multi-asperity contacts. *Proceedings of the Institution of Mechanical Engineers, Part J: Journal of Engineering Tribology, 223*, 767–776.

Johnson, K. L. (1987) *Contact mechanics*. Cambridge: Cambridge University Press.

Kalker, J., & Van Randen, Y. (1972). A minimum principle for frictionless elastic contact with application to non-Hertzian half-space contact problems. *Journal of Engineering Mathematics, 6*, 193–206.

Kosior, F., Guyot, N., & Maurice, G. (1999). Analysis of frictional contact problem using boundary element method and domain decomposition method. *International Journal for Numerical Methods in Engineering, 46*, 65–82.

Lai, W., & Cheng, H. (1985). Computer simulation of elastic rough contacts. *ASLE Transactions, 28*, 172–180.

Landenberger, A., & El-Zafrany, A. (1999). Boundary element analysis of elastic contact problems using gap finite elements. *Computers & structures, 71*, 651–661.

Liu, G., Zhu, J., Yu, L., & Wang, Q. J. (2001). Elasto-plastic contact of rough surfaces. *Tribology Transactions, 44*, 437–443.

Man, K., Aliabadi, M., & Rooke, D. (1993a). BEM frictional contact analysis: Load incremental technique. *Computers & structures, 47*, 893–905.

Man, K., Aliabadi, M., & Rooke, D. (1993b). BEM frictional contact analysis: Modelling considerations. *Engineering Analysis with Boundary Elements, 11*, 77–85.

Morales-Espejel, G. E., & Brizmer, V. (2011). Micropitting modelling in rolling–sliding contacts: Application to rolling bearings. *Tribology Transactions, 54*, 625–643.

Olukoko, O., Becker, A., & Fenner, R. (1993). A new boundary element approach for contact problems with friction. *International Journal for Numerical Methods in Engineering, 36*, 2625–2642.

Öqvist, M. (2001). Numerical simulations of mild wear using updated geometry with different step size approaches. *Wear, 249*, 6–11.

Oysu, C., & Fenner, R. (1998). Two-dimensional elastic contact analysis by coupling finite element and boundary element methods. *The Journal of Strain Analysis for Engineering Design, 33*, 459–468.

Poon, C., & Sayles, R. (1994). Numerical contact model of a smooth ball on an anisotropic rough surface. *Journal of Tribology, 116*, 194–201.

Ren, N., & Lee, S. C. (1993). Contact simulation of three-dimensional rough surfaces using moving grid method. *Journal of Tribology, 115*, 597–601.

Sahlin, F., Larsson, R., Almqvist, A., Lugt, P. M., & Marklund, P. (2009). A mixed lubrication model incorporating measured surface topography. Part 1: Theory of flow factors. *Proceedings of the Institution of Mechanical Engineers, Part J: Journal of Engineering Tribology, 224*, 335–351.

Sellgren, U., Björklund, S., & Andersson, S. (2003). A finite element-based model of normal contact between rough surfaces. *Wear, 254*, 1180–1188.

Sfantos, G. K., & Aliabadi, M. H. (2006a). Application of BEM and optimization technique to wear problems. *International Journal of Solids and Structures, 43*, 3626–3642.

Sfantos, G. K., & Aliabadi, M. H. (2006b). Wear simulation using an incremental sliding boundary element method. *Wear, 260*, 1119–1128.

Sfantos, G., & Aliabadi, M. H. (2007). A boundary element formulation for three-dimensional sliding wear simulation. *Wear, 262*, 672–683.

Thomson, R. A., & Bocchi, W. (1972). A model for asperity load sharing in lubricated contacts. *ASLE Transactions, 15*, 67–79.

Tonder, Y. Z., & Hu, K. (1992). Simulation of 3-D random rough surface by 2-D digital filter and Fourier analysis. *International Journal of Machine Tools and Manufacture, 32*, 83–90.

Tian, Xuefeng, & Bhushan, Bharat. (1996). A numerical three-dimensional model for the contact of rough surfaces by variational principle. *Journal of Tribology, 118*, 33–42.

Webster, M., & Sayles, R. (1986). A numerical model for the elastic frictionless contact of real rough surfaces. *Journal of Tribology, 108*, 314–320.

Willner, K. (2008). Fully coupled frictional contact using elastic halfspace theory. *Journal of Tribology, 130*, 031405.

Yamazaki, K., Sakamoto, J., & Takumi, S. (1994). Penalty method for three-dimensional elastic contact problems by boundary element method. *Computers & structures, 52*, 895–903.